Chinese Chemical Letters 33 (2022) 2585–2589

Contents lists available at ScienceDirect

Chinese Chemical Letters

journal homepage: www.elsevier.com/locate/cclet

Single-Cu-atoms anchored on 3D macro-porous carbon matrix as efficient catalyst for oxygen reduction and Pt co-catalyst for methanol oxidation

Jin Ma, Bin Liu, Rongyue Wang, Zhiyao Sun*, Ying Zhang, Yubo Sun, Zhuang Cai*, Yao Li, Jinlong Zou*

Key Laboratory of Functional Inorganic Material Chemistry, Ministry of Education of the People's Republic of China, School of Chemistry and Materials Science, Heilongjiang University, Harbin 150080, China

ARTICLE INFO

Article history:
Received 7 August 2021
Revised 26 August 2021
Accepted 16 September 2021
Available online 14 October 2021

Keywords:
Defects
Electrocatalytic activity
Macro-porous structure
Metal-nitrogen-carbon
Single atom catalyst

ABSTRACT

Single metal atoms immobilized on a carbon substrate are of great potential for enhancing the catalytic activities for oxygen reduction and methanol oxidation reactions (ORR/MOR) owing to the maximized atom utilization. Herein, single copper atoms (SCAs) are loaded on macro-porous nitrogen-doped carbon (Cu-NC) derived from zeolitic imidazolate framework-8 (ZIF-8), which are used as catalysts for ORR and Pt-supports for MOR. For ORR, the catalyst marked as Cu-NC-3 exhibits a higher peak potential of 0.87 V (*vs.* Reversible hydrogen electrode) than that of commercial Pt/C (0.83 V), mainly attributing to that the 3D macro-porous structure of Cu-NC-3 provides adequate space for uniform dispersion of SCAs as the main active species, and smooth diffusion pathways for fast transport of substances (O_2, H_2O), therefore reducing the overpotential and the intermediate (H_2O_2) generation to enhance ORR activity. For MOR, Pt-Cu-NC-3 has a higher mass activity of 1217.4 mA/mg_{Pt} than that of Pt/C (752.4 mA/mg_{Pt}), and its activity maintenance (decline of 27.6%) is also better than Pt/C (decline of 44.0%) after 5000 cyclic voltammetry (CV) cycles. The interactions between SCAs and Pt nanoparticles should facilitate the generation of OH^- from water molecules, which can fast eliminate the adsorbed CO to recover the Pt active sites to improve MOR performance. This synthesis strategy affords a new inspiration to prepare single metal atoms loaded on ZIFs-derived macro-structure with diverse activities for ORR/MOR.

To solve global energy and environmental problems, great efforts have been made to explore alternatives to fossil fuels [1–4]. Among the new energy sources, direct methanol fuel cell (DMFC) is one of the candidates to well meet the energy demand because of its advantages of clean fuel, simple cell structure, and fast start-up [5,6]. Although significant advances have been made in recent years, there are still obstacles to the commercialization of DMFC technology, including slow kinetics of anodic methanol oxidation reaction (MOR) and cathodic oxygen reduction reaction (ORR), high platinum (Pt) loading, easy catalyst poisoning, and serious agglomeration and corrosion of active components during catalytic process [7–9]. In general, Pt-based nanomaterials are considered as the most advanced catalysts for MOR/ORR [10]. However, Pt-based catalysts are difficult to be applied and commercialized on a large scale due to their exiguity, high price, low stability, and poor tolerance to carbon monoxide (CO)/methanol [11–13]. Therefore, it is urgent to develop non-noble metal-based catalysts with high activity, stability and resistance to toxicity.

Metal carbides have been used as non-noble metal catalysts in DMFCs by optimizing their geometric and electronic structures to improve their intrinsic activity and stability. In recent years, zeolite-imidazole frameworks (ZIFs) have become the hot raw materials to synthesize metal-nitrogen (N)-carbon catalysts [14–16]. Nevertheless, due to the limitation of such a fixed structure (polyhedron, sphere, *etc.*) of ZIFs-derived catalysts, the active sites on metal species cannot be fully utilized. Therefore, the size, structure and composition of these catalysts should be properly controlled to accelerate the electron transfer to further improve the electrocatalysis performance by allowing the barrier-free contact between active sites and reactants [17–19]. As reported previously, by comparing with the microporous electrocatalysts, the three-dimensional

* Corresponding authors.
E-mail addresses: zhiyao202@126.com (Z. Sun), hlju_chem218c@163.com (Z. Cai), zoujinlong@hlju.edu.cn (J. Zou).

https://doi.org/10.1016/j.cclet.2021.09.108
1001-8417/

(3D) macro-porous carbon matrix can expose the active sites to the maximum extent, thus significantly improving the diffusion of reactants (mass transfer) to obtain a higher electrocatalytic performance [20].

In addition to the improvement of mass transfer ability, it is particularly important to improve the utilization rate of active sites on the 3D macro-porous structure [21]. In particular, it is reported that by adding a small amount of metal single-atom species to the porous structure, higher catalytic selectivity and active-site availability can be obtained. There is no doubt that the single atoms-based catalysts are the best choices for electrocatalysis. At present, a series of monatomic metal catalysts, such as Pt, Co, Fe, *etc.*, have been studied in the field of electrochemistry [22–26]. As we all know, Cu as a low-cost metal usually has a comparable electrocatalytic activity to other transition metals (such as Fe, Co, Ni). Cu has the second highest conductivity, which is only lower than that of silver. This makes it possible to promote the charge transfer between the active sites and the reactants, which thus has a good effect on activity for electrocatalysis (oxygen evolution reaction (OER), *etc.*) [27–29]. Based on the above analyses, establishing a relationship between atomic (Cu) active sites and structural functions through a comprehensive method is a promising option for improving the catalytic activity for MOR/ORR.

This study reports the synthesis and application of single Cu atoms (SCAs) anchored on macro-porous carbon (Cu-NC) as catalysts for ORR and MOR (as Pt support). SiO_2 nanospheres as the template are added during the ZIF-8 synthesis process, which is completely removed by acid (HF) washing after carbonization to form a macro-porous carbon to facilitate the mass transfer. The reaction of copper nitrate trihydrate and urea occurs in a macro-porous medium to obtain the SCAs. As the temperature of the reaction solution rises under the ultrasound condition, the decomposition of urea in a high-energy environment can provide a weak alkaline environment for the reduction of Cu atoms. The well-dispersed SCAs can provide abundant active sites to enhance the adsorption of oxygen on the catalyst surface to improve the ORR performance. In addition, under the action of SCAs, Pt atom should correspondingly improve the catalytic activity and anti-toxicity (CO) in the MOR process. As expected, the as-prepared Cu-NC catalysts may exhibit higher catalytic activities, long-term durability and CO/methanol resistance than those of commercial catalysts for MOR and ORR.

The synthesis process of Cu-NC is schematically illustrated in Fig. 1a (The detailed preparation procedure, material characterizations and electrochemical tests can be seen in Supporting information). Fig. 1b shows that SiO_2 nanoparticles (NPs) are spherical shape with a narrow size range of 110 to 130 nm. $Zn(NO_3)_2{\cdot}6H_2O$ and 2-methylimidazole are coordinated to form to ZIF-8 to assemble with SiO_2 NPs. Abundant voids between SiO_2 NPs facilitate the deposition of ZIF-8 (Fig. 1c). ZIF-8 can interconnect the individual SiO_2 NPs through annealing for the formation of precursor material with SiO_2 NPs inside (Fig. 1d). As shown in Fig. S1 (Supporting information), the carbonized ZIF-8 NPs (without SiO_2, denoted as NC) still remain the original polyhedral morphology. NC-0 (without Cu source) is obtained by removing SiO_2 template from the carbon structure by using HF. The preparation processes of NC, NC-0, Pt-NC and Pt-NC-0 are provided in Supporting information. Macro-porous Cu-NC-3 catalyst with well-defined interconnections is obtained by adding Cu sources (Fig. 1e). The diameter of macropores is approximately 120 nm, which is similar to that of SiO_2 template, indicating that SiO_2 NPs have been completely washed away. The macro-porous structure with a high degree of 3D structural interconnection should facilitate the diffusion of the reactants and expose more active sites to significantly improve the stability of the catalysts (Fig. S2 in Supporting information). The high-angle annular dark-field-scanning transmission electron microscope (HAADF-STEM) image in Fig. 1f confirms that SCAs are well-dispersed on the surface of NC material. As shown in the inset of Fig. 1f (selected-area electron diffraction, SAED), the presence of several rings indicates the poor crystallinity of the prepared catalysts [30–32]. As shown in Figs. 1g-i (partially-enlarged mapping images), the C, N and Cu elements are uniformly dispersed in the NC skeleton. Notably, the uniform distribution of SCAs throughout the framework of NC can establish a large number of active sites, which will greatly promote the catalytic activity.

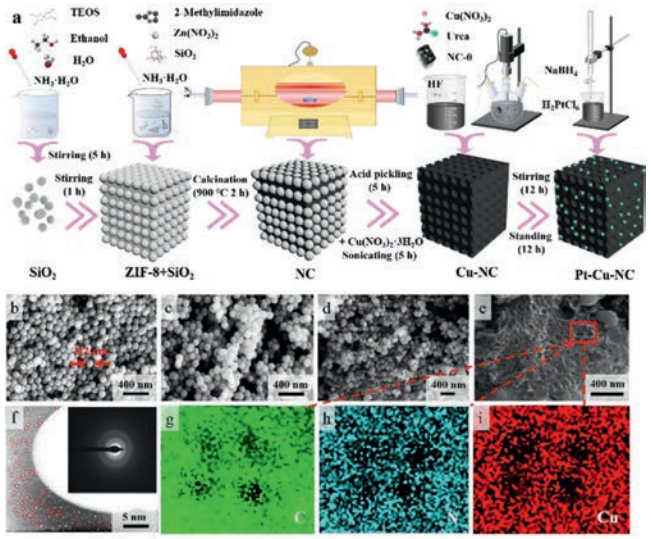

Fig. 1. (a) Schematic synthesis process for Cu-NC and Pt-Cu-NC composites. SEM images of silica (b), ZIF-8 -silica composite (c), ZIF-8-derived carbon-silica composite (d), and Cu-NC-3 (e). Atomic-resolution HAADF-STEM image of Cu-NC-3 material (f, SCAs show bright contrast), and the inset is the corresponding SAED pattern; elemental mapping results of C (g), N (h) and Cu (i).

As shown in Figs. 2a and b, N_2 adsorption-desorption isotherms for NC and Cu-NC-3 belong to type IV with H-3 hysteresis loops. There are a large number of mesopores and macropores in NC and Cu-NC-3 (S_{BET} of 315 m^2/g) as calculated by the Hamilton-Jacobi-Bellman (HJB) method. It confirms that macro-porous carbon (NC) with 3D structure is successfully prepared. The adsorption isotherms, specific surface area and pore size distributions of the Cu-NC-y (y = 1, 2, 4 and 5) catalysts are shown in Fig. S3 and Table S1 (Supporting information). The surface areas (S_{BET}) of Cu-NC catalysts with different Cu loadings do not differ much from each other. The larger S_{BET} of Cu-NC-2 and Cu-NC-3 indicates that more active sites (per unit mass) and mass transfer channels can be provided on the catalyst for reactants, thus promoting the transport of substances and the catalytic activity of the catalyst [33]. Moreover, the highly-porous structure can also provide enough space to obtain the uniform dispersion of SCAs.

As shown in Fig. 2c, the binding energies of Cu $2p_{3/2}$ are 932.3 and 934.8 eV, indicating that there are two chemical states Cu (Cu^+, Cu^{2+}) in Cu-NC-3 [34]. Two peaks at around 952.1 (Cu $2p_{1/2}$) and 954.6 eV (Cu $2p_{1/2}$) are attributed to Cu^+ and Cu^{2+}, respectively. The two peaks with relatively-weak intensities at around 943.7 and 963.0 eV correspond to the satellite peaks, which can be ascribed to the shakeup excitation [35]. The intensities of the satellite peaks are weak, indicating that Cu species is mainly existed in the form of single-atom with metallic state [32,34,36]. High-resolution X-ray photoelectron spectroscopy (XPS) spectra of Cu 2p for Cu-NC-y (y = 1, 2, 4 and 5) are shown in Fig. S4 (Supporting information). Fig. 2d and Fig. S5 (Supporting information) shows that the peaks at around 284.5, 285.4, 287.8, 288.9 and 291.7 eV correspond to C–C sp^2, C–O/C–N, C=O/C=N, O=C–OH and π-π^*, respectively. The largest peak areas of C–C sp^2 belong to the graphic car-

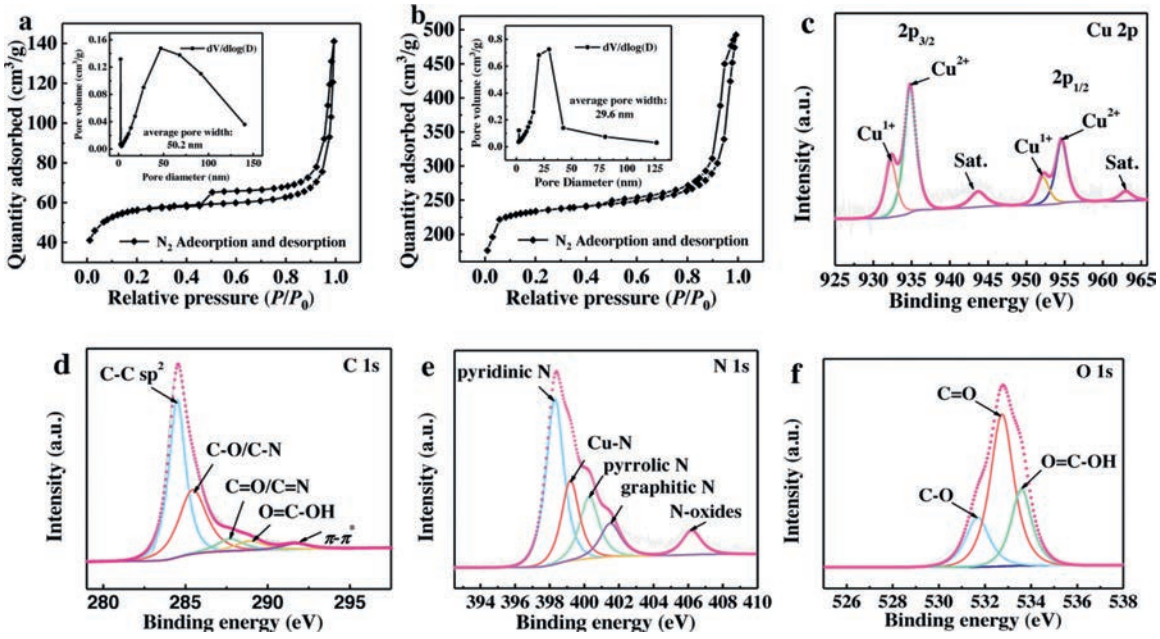

Fig. 2. N_2 adsorption/desorption isotherms and pore size distributions (inset) for NC (a) and Cu-NC-3 (b) catalysts. High resolution XPS spectra of Cu 2p (c), C 1s (d), N 1s (e), O 1s (f) for Cu-NC-3.

bon, indicating that the carbon skeleton is partially graphitized to obtain the promising conductivity [37]. Moreover, the existence of C–O/C–N and C=O/C=N shows that N atoms are successfully doped into the carbon skeleton. Both NC-0 and Cu-NC-*y* (y = 1, 2, 3, 4 and 5) have the peak of C=O/C=N, while NC does not show this peak (Fig. S5). The dipole moment of C=O/C=N is larger than that of C–O/C–N, indicating that C=O/C=N has a higher polarity to obtain a higher hydrophilicity [38,39]. The O=C–OH as an O-containing functional group on catalyst surface can also promote the surface hydrophilicity to facilitate the adsorption of H^+/O_2 to improve the ORR electrocatalytic activity [40].

In high-resolution XPS spectra of N 1s (Fig. 2e and Fig. S6 (in Supporting), there are five peaks at around 398.3, 399.1, 400.2, 401.5 and 406.2 eV correspond to pyridinic N, Cu-N, pyrrolic N, graphitic N and oxidized N, respectively. Pyridinic N can improve the O_2 adsorption capacity on adjacent C atoms to accelerate ORR electron transfer [41]. As reported previously, the coordination environment of Cu-N is the same as Cu phthalocyanine [34]. Pyridinic N can provide the coordination sites for central Cu atom to form Cu-N active sites implanted in carbon matrix [41]. π-π system of carbon is broken by graphitic N, which attracts electrons from adjacent carbon atoms to increase the adsorption capacity of O_2 [42]. As reported previously, oxidized N plays an important role in the process of decreasing protonation and increasing utilization of Pt *via* the charge-cloud interactions between Pt and oxidized N [43]. Because of the highest polarizability of oxidized N, it has been considered as the co-catalytic active-center for MOR [44]. Fig. 2f and Fig. S7 (Supporting information) show that the peaks at around 531.6, 532.7 and 533.5 eV correspond to O=C–OH, C=O and C–OH, respectively. A large number of surface oxygen-containing functional groups are generated on the carbon skeleton, which can promote the adsorption of oxygen, thereby improving the ORR catalytic activity.

In the X-ray diffraction (XRD) patterns (Fig. 3a), the peaks of graphitic carbon are observed at 2θ = 24.5°, and no other peaks appear because the Cu content is too small to be detected by XRD. As shown in the Raman spectra (Fig. 3b), peaks at around 1352 and 1590 cm^{-1} correspond to the D bands generated by lattice defects and the G bands generated by graphitic carbon, respectively.

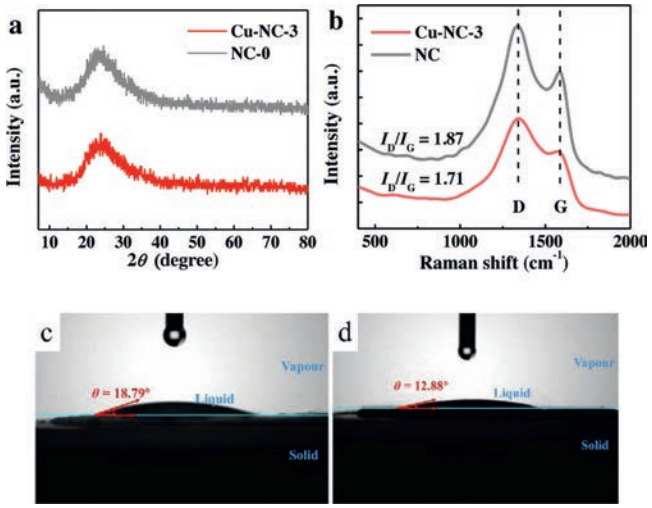

Fig. 3. XRD patterns of NC-0 and Cu-NC-3 (a); Raman spectra of NC and Cu-NC-3 (b); contact angles of NC (c) and Cu-NC-3 (d).

Cu-NC-3 has a lower I_D/I_G (1.71) value than that of NC (1.87), indicating that a higher degree of graphitization is obtained in Cu-NC-3. The conductivity and electronic transport ability of catalysts are enhanced with a high degree of graphitization. Stronger D band means that there are a lot of defects and vacancies in the as-prepared catalysts, which can provide more spaces for electrons to transfer, and also maximize the deposition of SCAs [32,45]. The contact angles of NC and Cu-NC-3 are 18.79° (Fig. 3c) and 12.88° (Fig. 3d), respectively, indicating that the catalyst shows a higher hydrophilicity. It is known that materials with polar groups have a great affinity for water [46], which makes the Cu-NC-3 catalyst more easily wetted by water. Therefore, the absorption time for electrolyte is shortened on the Cu-NC-3 catalyst, and then the contact between active sites and reactants is accelerated to improve the electrocatalytic performance.

In the O_2-saturated 0.1 mol/L KOH solution, the catalytic performances of Cu-NC-*y*, NC and Pt/C for ORR are examined. As shown

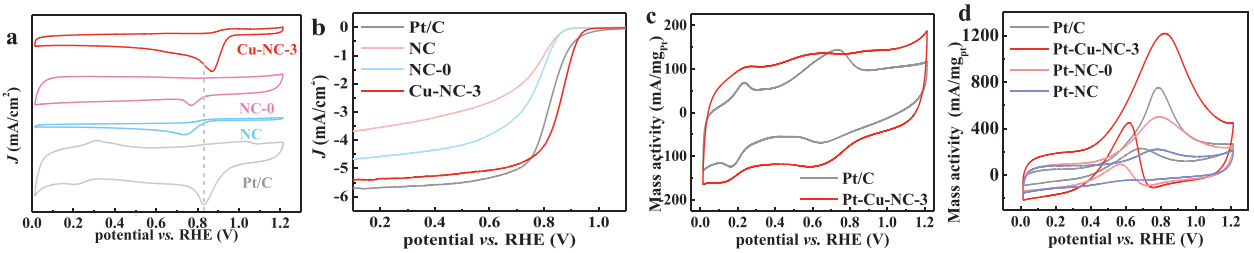

Fig. 4. CV curves for Pt/C, NC, NC-0 and Cu-NC-3 in an O_2-saturated 0.1 mol/L KOH solution at a scan rate of 10 mV/s (a); LSV curves (5 mV/s and 1600 rpm) in an O_2-saturated 0.1 mol/L KOH solution (b); CV curves of Pt-Cu-NC-3 and Pt/C tested in 1 mol/L KOH (c); CV curves of Pt-NC, Pt-NC-0, Pt-Cu-NC-3 and Pt/C catalysts in 1 mol/L KOH with 1 mol/L methanol at a scan rate of 50 mV/s (d).

in Fig. 4a and Fig. S8 (Supporting information), obvious oxygen reduction peaks are exhibited in cyclic voltammetry (CV) curves. Notably, Cu-NC-3 has the highest activity for ORR at peak potential of 0.87 V, which is much higher than those of commercial Pt/C (0.81 V), NC (0.73 V) and NC-0 (0.77 V). It implies that the proper loading of SCAs on the 3D macro-porous structure (Cu-NC-3) can form the Cu-N-C structure to greatly improve the ORR activity. Macro-porous carbon with a high degree of 3D structural interconnection can provide adequate space and diffusion pathways for transport of substances (O_2, H_2O, OH^-) and facilitate the uniform dispersion of the crucial Cu-N active sites [45]. According to previous reports, the adsorption energy of Cu^{2+}-N (bridge-connected) for oxygen is extremely close to that of commercial Pt/C [32,34]. According to the Sabatier principle [47], it is believed that Cu^{2+}-N is the main active site of Cu-NC-3 for ORR. LSV tests are conducted at a rotating speed of 1600 rpm to estimate ORR activity in O_2-saturated 0.1 mol/L KOH electrolyte. In Fig. 4b and Fig. S9 (Supporting information), Cu-NC-3 shows better onset potential (E_0 = 0.95 V), half-waves potential ($E_{1/2}$ = 0.87 V) and limiting current density (J_L = 5.4 mA/cm^2) than those of Pt/C (E_0 = 0.92 V, $E_{1/2}$ = 0.84 V and J_L = −5.7 mA/cm^2). Table S2 (Supporting information) shows the ORR activities of Cu-NC-3 and other recently-reported transition metals-based catalysts. More ORR test results are provided in Figs. S10–13 (Supporting information).

Fig. 4c shows the CV curves of Pt-Cu-NC-3 and Pt/C tested in 1 mol/L KOH solution. The electrochemical activity surface area (ECSA) of Pt-Cu-NC-3 (150.1 m^2/g$_{Pt}$) can be obtained by calculating the area of the hydrogen zone in the CV curve, which is much greater than that of Pt/C (93.9 m^2/g$_{Pt}$). The larger hydrogen adsorption and desorption areas of the catalysts, the larger ECSA and the higher MOR activity [46]. Pt-Cu-NC-3 has a larger hydrogen adsorption and desorption area, mainly because the 3D macro-porous structure can fully utilize the Pt active sites, thereby improving the MOR performance [48]. As shown in Fig. 4d, Pt-Cu-NC-3 has a high mass activity of 1217.4 mA/mg$_{Pt}$ at 0.8 V (50 mV/s), which is much higher than that of Pt/C (752.4 mA/mg$_{Pt}$). In addition, the mass activity of Pt-NC-0 (501.8 mA/mg$_{Pt}$) is also higher than that of Pt-NC (221.4 mA/mg$_{Pt}$). Fig. S14 (Supporting information) shows that the mass activities of Pt-Cu-NC-y (y = 1, 2, 4 and 5) are 718, 919.2, 878.6, and 527 mA/mg$_{Pt}$, respectively. The macro-porous structure of Cu-NC-y supports can improve the utilization of Pt to promote the mass activity [45]. Table S3 (Supporting information) compares the MOR activity of Pt-Cu-NC-3 with other similar catalysts that have been recently reported. It shows that Pt-Cu-NC-3 exhibits the highest mass activity. The SCAs that form the catalytically active sites are usually combined with non-metallic N atoms [36]. When there are other metals (such as Pt) around, it may cause the metal atomic orbital to overlap and form a complicated effect [49]. The interactions between two atoms (Pt and Cu) can cause the redistribution of electrons to catalyze the *OH generated by water molecules in the electrolyte, which can fast react with the intermediates such as CO to release the active sites to improve MOR performance [36,50]. More MOR test results are provided in the Supporting information (Figs. S15–18 in Supporting information). The schematic illustration of possible mechanisms for ORR (Cu-NC-3) and MOR (Pt-Cu-NC-3) is shown in Fig. 5, and more discussions are provided in Supporting information.

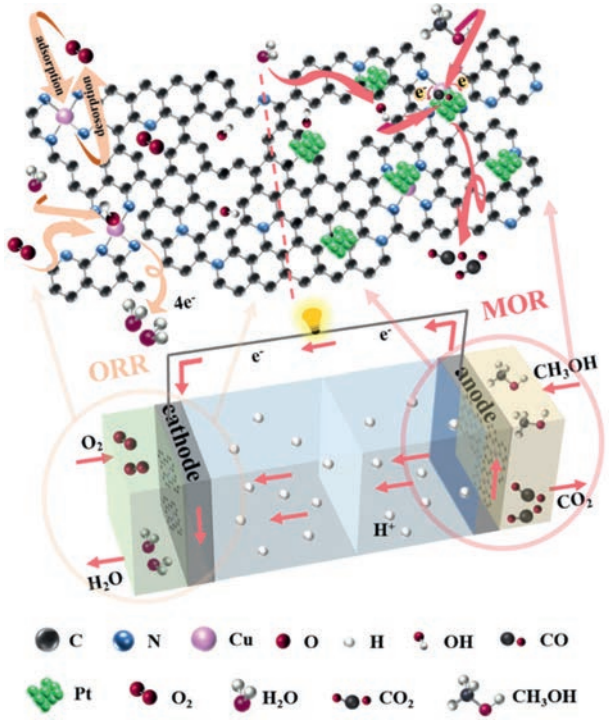

Fig. 5. Schematic illustration of possible mechanisms for ORR (Cu-NC-3) and MOR (Pt-Cu-NC-3).

In summary, we present a new approach for synthesis of Cu-NC composites from ZIF-8 as highly active catalysts with a promising tolerance to methanol for ORR and as Pt-supports with a superior CO tolerance for MOR. Cu-NC-3 has the highest ORR activity with a peak potential of 0.87 V, E_0 = 0.95 V, $E_{1/2}$ = 0.87 V and J_L = 5.4 mA/cm^2. Cu-NC-3 shows better Tafel slopes and R_{ct} value than those of commercial Pt/C. Such an excellent ORR performance of Cu-NC-3 is achieved by using the SCAs as the active species loaded on the N-containing defective carbon matrix. Moreover, Pt-Cu-NC-3 has higher mass activity (1217.4 mA/mg$_{Pt}$), CO tolerance, and stability than those of Pt/C, which is attributed to that the strong interactions between SCAs and Pt NPs allow electrons to be accumulated around Pt atom to improve catalytic activity and stability. In this study, we rationally design a highly-active ORR/MOR catalyst/co-catalyst with a promising stability, and pro-

vide a deeper understanding of the synergy between the single atoms and the 3D structure of carbon matrix. In the future, single atoms-based catalysts will continue to attract a great deal of attention because of their maximal atom utilization and, more importantly, promising activity and selectivity toward various reactions.

Declaration of competing interest

The authors declare that they have no known competing financial interests or personal relationships that could have appeared to influence the work reported in this paper.

Acknowledgments

We acknowledge the support by the National Natural Science Foundation of China (Nos. 52070074, 21806031 and 51578218), Longjiang Scholars Program (No. Q201912), and the Open Project of State Key Laboratory of Urban Water Resource and Environment, Harbin Institute of Technology (No. HC202144).

Supplementary materials

Supplementary material associated with this article can be found, in the online version, at doi:10.1016/j.cclet.2021.09.108.

References

[1] J.B. Dunn, E. Newes, H. Cai, Energy Environ. Sci. 13 (2020) 2262–2274.
[2] Y. Li, H. Wang, C. Priest, Adv. Mater. 33 (2021) 2000381.
[3] N. Uddin, H.Y. Zhang, Y.P. Du, Adv. Mater. 32 (2020) 1905739.
[4] G. Yilmaz, S.B. Peh, D. Zhao, Adv. Sci. 6 (2019) 1901129.
[5] M. Liu, Z. Zhao, X. Duan, Adv. Mater. 31 (2019) 1802234.
[6] S. Mohanapriya, S.D. Bhat, A.K. Sahu, Energy Environ. Sci. 2 (2009) 1210–1216.
[7] X. Li, Y.M. Liu, W. Bi, J. Mater. Chem. A 8 (2020) 16477–16486.
[8] H. Xu, H.Y. Shang, C. Wang, Adv. Funct. Mater. 30 (2020) 2000793.
[9] L. Zhang, P.P. Lu, Y.R. Luo, J. Mater. Chem. A 9 (2021) 9609–9615.
[10] H. Jeong, D. Shin, B.S. Kim, Angew. Chem. Int. Ed. 59 (2020) 20691–20696.
[11] A. Beniya, S. Higashi, N. Ohba, Nat. Commun. 11 (2020) 1888.
[12] L.H. Liang, H.H. Jin, H. Zhou, Nano Energy 88 (2021) 1066221.
[13] M. Yoo, Y.S. Yu, H. Ha, Energy Environ. Sci. 13 (2020) 1231–1239.
[14] Y. Arafat, M.R. Azhar, Y. Zhong, Adv. Energy Mater. 11 (2021) 2100514.
[15] X. Feng, Y. Bai, M.Q. Liu, Energy Environ. Sci. 14 (2021) 2036–2089.
[16] Y.Y. Li, P.Y. Zhang, L.Y. Wan, Adv. Funct. Mater. 31 (2021) 2009645.
[17] J.J. Ban, X.H. Wen, H.J. Xu, Adv. Funct. Mater. 31 (2021) 2010472.
[18] C.X. Tang, Z.L. Feng, X.F. Bai, Fuel 302 (2021) 121186.
[19] W. Wang, B. Xu, X. Pan, Angew. Chem. Int. Ed. 60 (2021) 7802–7808.
[20] H.S. Kim, C.H. Lee, J.H. Jang, J. Mater. Chem. A 9 (2021) 4297–4309.
[21] H.W. Zhao, Y.Q. Zhang, L.X. Li, Chin. Chem. Lett. 32 (2021) 140–145.
[22] L.L. Chen, X.L. Xu, W.X. Yang, J.B. Jia, Chin. Chem. Lett. 31 (2020) 626–634.
[23] H.J. Cho, D. Kim, J. Li, J. Am. Chem. Soc. 140 (2018) 13514–13520.
[24] I. Kone, Z. Ahmad, A. Xie, Energy Technol. 8 (2020) 2000409.
[25] J.J. Shi, X.X. Shu, C.S. Xiang, J. Mater. Chem. A 9 (2021) 6861–6871.
[26] Y.M. Wang, E.G. Luo, X. Wang, Chin. Chem. Lett. 32 (2021) 506–510.
[27] Z. Cai, S. Lin, J. Xiao, Small 16 (2020) 2002518.
[28] Y. He, Q. Shi, W. Shan, Angew. Chem. Int. Ed. 60 (2021) 9516–9526.
[29] X.H. Liu, X.W. Zhai, W.B. Sheng, J. Mater. Chem. A 9 (2021) 10110–10119.
[30] M.O. Cichocka, Z. Liang, D. Feng, J. Am. Chem. Soc. 142 (2020) 15386–15395.
[31] B.L. Li, Z.S. Li, Q. Pang, Chem. Eng. J. 401 (2020) 126045.
[32] T.T. Sun, Y.L. Li, T.T. Cui, Nano Lett. 20 (2020) 6206–6214.
[33] A.I. Douka, Y. Xu, H. Yang, Adv. Mater. 32 (2020) 2002170.
[34] W. Li, C. Min, F. Tan, ACS Nano 13 (2019) 3177–3187.
[35] A. Marciniak, S. Marcantoni, F. Giusti, Nat. Phys. 17 (2021) 1–6.
[36] D.H. Wang, C.C. Ao, X.K. Liu, ACS Appl. Energy Mater. 2 (2019) 6497–6504.
[37] Y. Zhang, Y.B. Sun, Z. Cai, J. Colloid Interface Sci. 593 (2021) 345–358.
[38] G. Hong, Y. Han, T.M. Schutzius, Nano Lett. 16 (2016) 4447–4453.
[39] J. Surgailis, A. Savva, V. Druet, Adv. Funct. Mater. 31 (2021) 2010165.
[40] J.H. Li, S.J. You, M.Y. Liu, Appl. Catal. B: Environ. 265 (2020) 118574.
[41] C. Huang, L.R. Zheng, W.S. Feng, ACS Sustain. Chem. Eng. 8 (2020) 14030–14038.
[42] W.J. Zang, T. Yang, H.Y. Zou, ACS Catal. 9 (2019) 10166–10173.
[43] N.K. Chaudhari, Y.G. Hong, B. Kim, J. Mater. Chem. A 7 (2019) 17183–17203.
[44] X. Peng, D. Chen, X. Yang, ACS Appl. Mater. Interfaces 8 (2016) 33673–33680.
[45] S. Chen, D.M. Huang, D.Y. Liu, Appl. Catal. B: Environ. 291 (2021) 120065.
[46] Y.B. Sun, Y. Li, S.J. You, Chem. Eng. J. 424 (2021) 120065.
[47] B.Z. Lu, Q.M. Liu, S.W. Chen, ACS Catal. 10 (2020) 7584–7618.
[48] A. Yuda, A. Ashok, A. Kumar, Catal. Rev. 62 (2020) 81–103.
[49] J.R. Yang, W.H. Li, D.S. Wang, Y.D. Li, Adv. Mater. 32 (2020) 2003300.
[50] X.J. Cui, H.Y. Su, R.X. Chen, et al., Nat. Commun. 10 (2019) 1–8.